The Kuroshio East of Taiwan: Modes of Variability and Relationship to Interior Ocean Mesoscale Eddies

DONGXIAO ZHANG,* THOMAS N. LEE, AND WILLIAM E. JOHNS

Rosenstiel School of Marine and Atmospheric Science, University of Miami, Miami, Florida

CHO-TENG LIU

Institute of Oceanography, National Taiwan University, Taipei, Taiwan

RAINER ZANTOPP

Rosenstiel School of Marine and Atmospheric Science, University of Miami, Miami, Florida

(Manuscript received 24 June 1999, in final form 12 July 2000)

ABSTRACT

Observations from the World Ocean Circulation Experiment PCM-1 moored current meter array in the East Taiwan Channel are analyzed and combined with TOPEX/Poseidon altimetry data and the Parallel Ocean Climate Model simulation to study Kuroshio variability and relationships to westward propagating sea surface height anomalies in the Philippine Sea.

Approximately 60% of the total subinertial velocity and temperature variance in the Kuroshio east of Taiwan is associated with so-called ''transport'' and ''meandering'' modes revealed from empirical orthogonal function analysis. The transport mode is dominated by a 100-day peak, while the most coherent energetic meandering signals are found in three limited frequency bands centered near periods of 100 days, 40 days, and 18 days. The detailed structure of the meanders is studied by frequency domain EOF analysis, which also reveals a higher frequency meander centered near 10 days confined to the western side of the channel.

On the 100-day timescale, the Kuroshio transport entering the East China Sea is strongly related to meandering of the Kuroshio, which in turn is caused by westward propagating anticyclonic eddies from the interior ocean. During low transport events, the Kuroshio meanders offshore and partly bypasses the East Taiwan Channel to flow northward along the eastern side of the Ryukyu islands. The interior eddy features that lead to the meandering can be identified as far east as 134°E, propagating westward to the coast of Taiwan at about 10 km day^{-1}. The 100-day variability that is so dominant in the Kuroshio is virtually absent in the Florida Current but is strongly present east of Bahamas in the Antilles Current and deep western boundary current, presumably being blocked from entering the Straits of Florida by the Bahamas Island chain.

1. Introduction

The Kuroshio originates to the east of the Philippines, where the North Equatorial Current bifurcates into the northward flowing Kuroshio and southward flowing Mindanao Current. As the western boundary current of the North Pacific subtropical gyre, it flows close to the east coast of Luzon and Taiwan before entering the East China Sea (ECS) through the channel formed by the northeast coast of Taiwan and Japanese Ryukyu Islands at about 24.5°N (Fig. 1). As a point of reference, this channel is designated as the East Taiwan Channel (ETC) in this paper. The Kuroshio and its analogous current in the North Atlantic, the Gulf Stream, influence the climate variation in the Northern Hemisphere by transporting warm waters from the tropical regions to the high-latitude regions. The ETC confines the Kuroshio in similar fashion to the Gulf Stream (Florida Current) confinement within the Straits of Florida. However, unlike the Gulf Stream whose mean transport and seasonal variation have been well-established as 31.7 ± 3 Sv (Sv ≡ 10^6 m^3 s^{-1}) from a series of dropsonde and current meter array measurements in the Straits of Florida (Schmitz and Richardson 1968; Molinari et al. 1985; Leaman et al. 1987; Schott et al. 1988), the mean transport and variability of the Kuroshio remain relatively controversial, and represent one of the major uncertain-

* Current affiliation: NOAA Pacific Marine Environmental Laboratory, Seattle, Washington.

Corresponding author address: Dr. Dongxiao Zhang, NOAA/Pacific Marine Environmental Laboratory, 7600 Sand Point Way NE, Seattle, WA 98115.
E-mail: zhang@pmel.noaa.gov

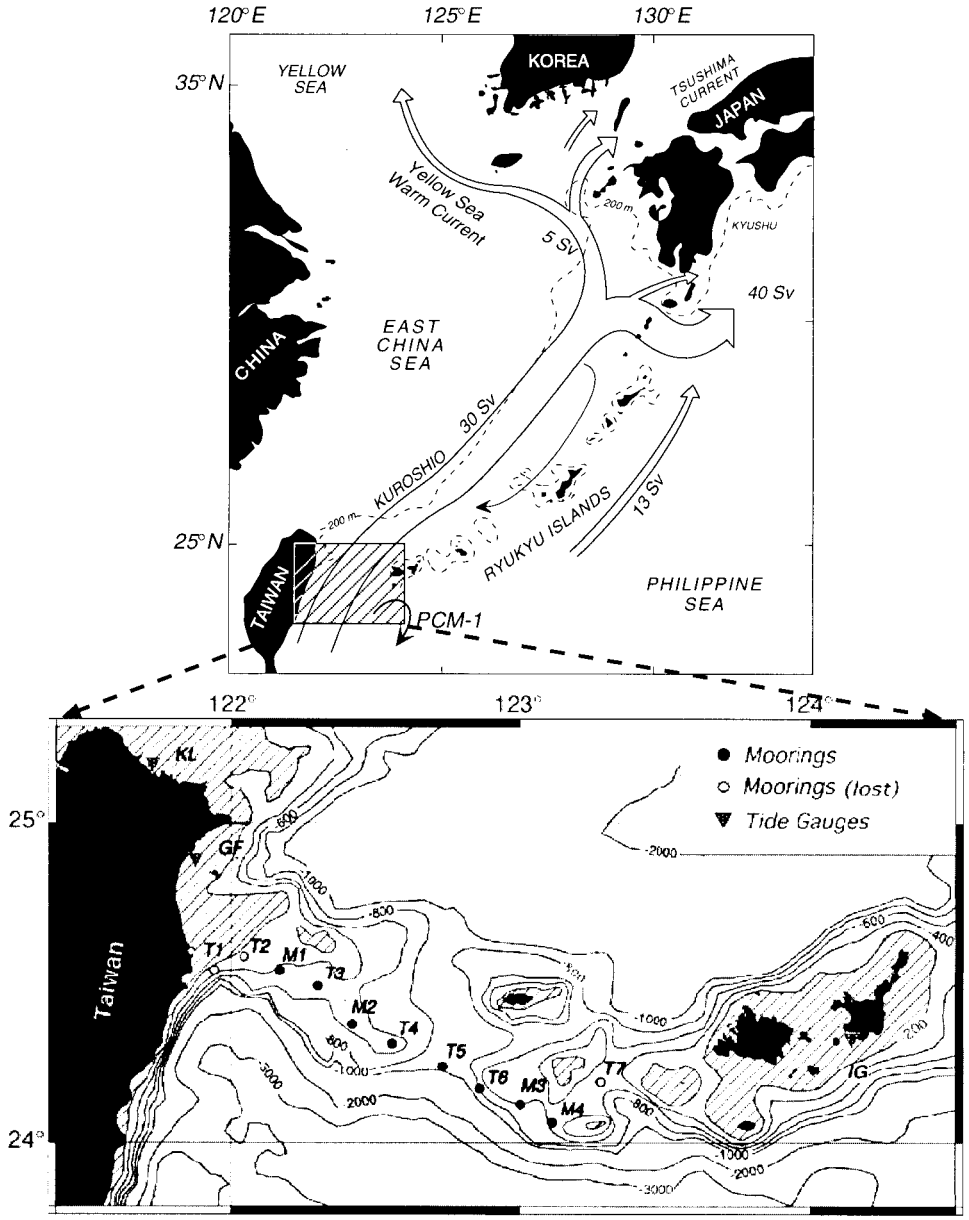

FIG. 1. (a) Schematic of the western boundary currents with estimated mean transports in the vicinity of the East China Sea (after Nitani 1972). The striped area east of Taiwan marks the East Taiwan Channel, where the WOCE PCM-1 moored current meter array was deployed. (b) Moorings and tide gauge locations on the topography of the Ilan Ridge. Shaded area indicates depth less than 200 m.

ties in estimating the net meridional transpacific heat flux across the midlatitude.

Historical investigations suggest a wide range of the Kuroshio transport estimates in the ECS from a minimum of about 15 Sv to a maximum of near 50 Sv (e.g., Nitani 1972; Konaga et al. 1980; Guan 1983). The transport has often been reported to change by more than 50% in two consecutive shipboard section surveys, sometimes by 2–3 months apart. Estimates of the mean transport vary from 21 to 33 Sv (Nitani 1972; Guan 1981, 1983; Roemmich and McCallister 1989; Bryden et al. 1991; Bingham and Talley 1991; Ichikawa and Beardsley 1993). The seasonal cycle is reported to be semiannual with maximum flow in spring and late winter and minimum in early summer and fall with an annual range of 7 Sv (Guan 1981), but Ichikawa and Beardsley (1993) show an annual range of 20–30 Sv with maximum in summer. All these previous estimates of the volume transport were based on snapshots from hydrographic surveys, and the accuracy of the calculated transport depends critically on the hydrographic sampling patterns, temporal aliasing noise, and the accuracy

of the zero velocity level assumption, or the reference velocity if available, the last one depends on the degree to which the shipboard-measured currents are influenced by tides.

Recent current meter observations from the World Ocean Circulation Experiment PCM-1 moored array in the ETC revealed that the mean Kuroshio volume transport was 21.5 ± 2.5 Sv with an annual range of 4 Sv, but the dominant current and transport variability occurred on 100-day timescales with amplitudes up to 8–12 Sv (Johns et al. 2001). The spectra of the transport time series also showed secondary peaks in period bands 12–22 and 30–40 days. Variations of transport in the ECS within the two shorter period bands were previously reported by Ichikawa and Beardsley (1993) based on the comparison of Kuroshio transport between hydrographic transects in the northern ECS. Their results indicated short and small-scale wavelike fluctuations in Kuroshio transport with an approximate amplitude of 5–10 Sv, period of 8–32 days, wavelength of 150–375 km, and downstream phase velocity of 8–19 km day^{-1}. These fluctuations have characteristics similar to those of Kuroshio frontal meanders. Qiu et al. (1990) analyzed consecutive satellite images and found that dominant meanders of Kuroshio in the ECS typically have wavelengths of 100–200 km, periods of 14–20 days, and downstream phase speeds of 17–22 km day^{-1}. Recent results from an inverted echo sounder array across the Kuroshio in the ECS also show evidence of energetic meanders with periods of 7, 11, and 16 days (James et al. 1999).

In the ECS, the warm saline water of the Kuroshio meets the cooler and fresher coastal water along the continental shelf break, modifying the properties of both waters by their interactions. These interactions affect not only the biological process and sediment distribution in the ECS, but also the heat and freshwater balance of the North Pacific. Similar to that occurring along the South Atlantic Bight (SAB) in the northwest Atlantic Ocean (Lee et al. 1991; Miller and Lee 1995), meanders and frontal eddies are believed to be important in these interactions. Numerical studies (Miller and Lee 1995) in the SAB suggest that the meandering processes are sensitive to the upstream meander patterns near the northern end of the Straits of Florida. The variability and meandering of the Kuroshio in the PCM-1 section, which serves as an entry of the Kuroshio into the ECS, may also play an important role in the downstream meander propagation and the upwelling and mixing processes in the ECS. A full understanding of the Kuroshio variation at this section has therefore considerable importance for better understanding and modeling the physical processes in the ECS.

The WOCE PCM-1 moored current meter array, deployed at the entrance of the Kuroshio into the ECS, is the first direct current observation that spans the width and depth of the Kuroshio. It provides an opportunity to determine the dominant Kuroshio transport and structure variations. In this paper, we will introduce two dominant modes of the Kuroshio structure that are related to the energetic transport fluctuations, particularly on the 100-day timescale. These two modes are found to result from the large Kuroshio meanders upstream of the PCM-1 array. Further investigation of the mesoscale variability over a larger domain, including the Philippine Basin using the TOPEX/Poseidon (T/P) altimetry data, reveal the links between the Kuroshio meander and the arrival of westward propagating mesoscale eddies from the interior ocean.

The structure of this paper is summarized as follows. A description of the PCM-1 observations and the methods used to derive the cross-stream velocity and temperature fields, as well as the objective analysis (OA) scheme (Mariano and Brown 1992) used to map the T/P altimetry onto regular grids in the study region is first given in section 2. Section 3 illustrates the Kuroshio mean vertical structure and temporal variations. We then show in section 4 that 60% of the current variation over the PCM-1 array is contained in two dominant EOFs that can be interpreted as transport and meandering modes. The transport mode is dominated by a 100-day fluctuation while the meandering mode is energetic at limited period bands of 70–200 days, 30–40 days, and 12–22 days. These meanders are further analyzed by using frequency domain EOF analysis on the three bands to show their detailed spatial structures and phase variations. In section 5, we show how the Kuroshio transport fluctuations are related to the large meanders. Section 6 compares these results with the variations of the Kuroshio simulated by the Parallel Ocean Climate Model (POCM) (Semtner and Chervin 1992; Stammer et al. 1996), followed by a summary and discussion section.

2. Observations and data processing

a. PCM-1 array

Current velocity observations were collected from a current meter array moored in the ETC between September 1994 and May 1996 (referred to as the PCM-1 array) as part of the World Ocean Circulation Experiment. The ETC is formed by the Ilan Ridge (Fig. 1) between the east coast of Taiwan and the southern Ryukyu island of Iriomote with a maximum depth of 1000 m, and it serves as a sill and choke point for Kuroshio flowing into the ECS. Downstream of the ridge is Okinawa Trough (2000 m deep) and upstream is the western Philippine Sea (depths reaching 4000 m).

The PCM-1 array consisted of 11 moorings (M1–M4 and T1–T7) distributed along the upstream flank of the Ilan Ridge to minimize the potential topographic shielding or steering of the flow as it navigates through the complex topography. Moorings M1–M4 were constructed by the University of Miami and moorings T1–T7 (T1, T2, and T7 were lost due to fishing activities) by the National Taiwan University. In addition to conven-

tional VACM and Aanderaa current meters, moorings T3 and T4 contained upward-looking 150-kHz acoustic Doppler current profilers (ADCPs) mounted at 350–400 m depth. Moorings M1 and M3/M4 bracketing the main channel included extra temperature and conductivity sensors along the mooring line and bottom pressure gauges to allow them to function as ''dynamic height'' moorings. Moorings T5 and T6 also contained deep current meters to measure the flow below 500 m entering the deep central gap of the channel.

All conventional current meters measured temperature in addition to current speed and direction, and at least one of the upper current meters on each mooring measured pressure to keep track of vertical mooring motion. Mooring T3 was out of service for refurbishment from May to October 1995 and mooring T4 was retrieved and not redeployed after May 1995. Detailed descriptions of mooring deployment and data recovery can be found in Johns et al. (2000). The most complete data coverage period was from September 1994 to May 1995 when both ADCPs on T3 and T4 were in service; we refer to this time period as period A. The cross-sectional distribution of instruments that returned velocity and temperature data is superimposed on the contoured mean and standard deviation of velocity and temperature fields in Fig. 2. The influence of lost instrumentation and the effort to fill these data gaps are described by Johns et al. (2001).

This paper uses the cross-sectional fields of u, v, and T on a 5 km (in horizontal) and 25 m (in vertical) grid. These fields are derived from records that were low-pass filtered with a 40-h Lanczos window and subsampled at 12-h intervals. Horizontal currents have been rotated by 30° so that v is downstream and perpendicular to the alignment of the array, u is positive toward the east along the PCM-1 orientation. To derive the T structure, a vertical temperature gradient $dT/dp(T)$ was first constructed for each mooring location, using climatology data from historical CTD casts taken in the vicinity of the moorings. This temperature gradient was then combined with the measured temperatures by integrating upward and downward from adjacent measurement points on the mooring and forming a weighted average of these estimates at the discretized vertical levels [see Johns et al. (2000) for details]. Above the highest measurement level on the mooring, the integration is carried upward until either the surface is reached or the predicted temperature exceeds the climatological (monthly) sea surface temperature for that location, in which case the integration is stopped and a mixed layer is added to the top of the profile at the monthly SST. This method was used to generate the vertical temperature profiles for the total water column at M1–M4, and partial profiles at T5 and T6 to a height of 150 m above the top measurement. These temperature time series at discretized vertical levels and the available direct temperature measurements from T3 and T4 were mapped onto the grid across the channel using the combined Laplacian and spline interpolation/extrapolation scheme. The v fields were generated by the so-called ''adjusted geostrophic method'' in Johns et al. Specifically, it uses dynamic height profiles, derived from the T fields and climatological T–S relationships, to estimate the baroclinic shear field of v across the entire channel. These velocity profiles at the mooring locations, referenced to the observed 400-m velocity, are substituted for any lost measurements, after which all records available at each time step (either from direct measurements or from geostrophic estimation) are interpolated to generate a final v field. For example, at mooring T4, in period A when the ADCP measurements were available, the directly measured v profiles at this location were used; whereas when T4 was out of service, geostrophic profiles were inserted. The discussion and evaluation of this technique is given by Johns et al. (2000), showing that the indirectly estimated geostrophic velocities offer a useful approximation of real velocities and produce consistent transport estimates when compared to direct methods. The cross-channel u fields were directly interpolated onto the grid from the direct measurements in September 1994–May 1995. Unlike in the derivation of v fields by using the adjusted geostrophic method, the lack of measurements in the central part of the channel after the retrieval of the ADCP on mooring T4 makes the construction of complete u fields impossible after May 1995. In general, we can derive reliable T and v fields during the entire PCM-1 observation period, and u fields during period A.

b. Satellite data

The sea level height observations (collinear data) collected by the TOPEX/Poseidon (T/P) altimeter from cycle 1 to cycle 194 (23 Sep 1992–29 Dec 1997) are used in this study. The focus region is on the Philippine Sea from 18° to 35°N and from the east Taiwan coast to 142°E. The raw altimetry data are corrected for the solid earth tide, wet and dry tropospheric range delay, atmospheric loading, and electromagnetic bias using the standard output from the geophysical data record (Callahan 1993). Unrealistic slopes (cross track slope > 10 cm km^{-1}) are excluded from the dataset. The data are flagged where the depth of ocean is shallower than 200 m or tides of Schrama and Ray (1994) are more than 5 cm different than the University of Texas tide model. The above processing was completed by the NASA Ocean Altimeter Pathfinder Project at Goddard Space Flight Center. The mean sea level is then removed from the dataset, leaving the sea surface height anomaly (SSHA) as the database for the present study.

In order to account for the mesoscale features present in this area, the objective analysis (OA) scheme of Mariano and Brown (1992) was used to map the SSHA onto a 0.25° lat × 0.25° long grid every 5 days. The following anisotropic and time-dependent correlation model,

$$C(dx, dy, dt) = C_1[1 - (Dx/C_4)^2 - (Dy/C_5)^2] \times \exp\{-[(Dx/C_6)^2 + (Dy/C_7)^2 + (dt/C_8)^2]\} \quad (1)$$

$$Dx = dx - C_2 dt \quad (2)$$

$$Dy = dy - C_3 dt, \quad (3)$$

was used, where dx, dy, and dt are the east–west, south–north, and temporal lags, respectively. The eight parameters in the above formula are listed and explained in Table 1. The phase speed C_2 is predetermined as the lowest translation speed of the mesoscale features in the investigation domain using the calculated covariance fields of SSHA [similar to Fig. 3 in Gilson et al. (1998)] measured by T/P in this region. Here C_2 serves as carrying the information to the past and future points with a rather fast degradation by $e^{-(dt/C_8)^2}$. It therefore would not create artificial features but give a rather realistic estimate of the shape of mesoscale eddies.

3. Mean flow and variability statistics

In this section we present the statistical properties and the temporal evolution of the Kuroshio at the ETC as observed by the PCM-1 array during the 21-month period. Figures 2a–f show the cross-stream structure of the mean u, v, and T fields (a–c) and the standard deviations of these variables (d–f), together with instrument configuration and section topography. The ETC is mostly contained between M1 and M4, considering the shallow banks that extend from the east Taiwan coast to M1 and from M4 to Iriomote. In fact, as long as the Kuroshio axis is in its normal direction, perpendicular to the PCM-1 array, the partial section between M4 and Iriomote is redundant, because it is in the downstream direction from M4 (Fig. 1). The mean u field is characterized by a weak eastward flow over the entire section with a maximum core of 5 cm s^{-1} near the bottom on the western side of the channel. This appears to be caused by the topographic constriction of the shallow bank of less than 200 m downstream of the PCM-1 moorings M2 and T3 (Fig. 1). Consistent with historical hydrographic measurements (Nitani 1972; Liu et al. 1998), the mean downstream velocity (Fig. 2b) shows clearly a velocity maximum of 100 cm s^{-1} in the western part of the channel, with the core tilted to the anticyclonic side of the current as depth increased. This feature is similar to the mean downstream velocity structures of Gulf Stream in the Straits of Florida (Leaman et al. 1987) and to the east of Cape Hatteras (Halkin and Rossby 1985; Johns et al. 1995b).

The u field is characterized by large standard deviations (Fig. 2d) that increase toward the east and the surface and are comparable to the standard deviation of the v field along the entire section. The v standard deviation tends to be more zonally uniform with a weak maximum of 35 cm s^{-1} slightly shoreward of the mean downstream velocity core. The large T standard deviations in the surface layer are caused by seasonal heating and cooling. Nevertheless, peak values of the T standard deviation (Fig. 2f) are found near 100-m depth at the western mooring M1 and extend along the main thermocline to the eastern and deeper part of the channel. All these features are consistent with the energetic meanders to the east of Taiwan that will be discussed in section 4.

Figures 3a, 3b, and 3c describe the time evolution of 100-m downstream velocity, the Kuroshio transport, and 300-m temperature measured by the PCM-1 array. The downstream velocity of Kuroshio fluctuates energetically with the current axis shifting onshore and offshore in the ETC (Fig. 3a). For instance, from late September to early November 1994, the current axis migrates offshore to the midchannel and onshore back to its normal position within 40 days. Associated with these onshore and offshore meanders were cross-sectional warming and cooling due to the migration of the sloping temperature front back and forth across the channel (Fig. 3c). Perhaps most striking are the pulses of weak currents across the entire ETC that occurred in March 1995, June 1995, October 1995, January 1996, and May 1996. Comparison of Figs. 3a and 3b illustrates that low transport events responsible for the 100-day transport fluctuations are associated with these pulses, all of which (except the June 1995 event) were preceded by onshore shifts of the current axis. Although the Kuroshio offshore meandering is not clear in the v fields of Fig. 3 after the onshore shift, the offshore displacement of the Kuroshio is strongly suggested by the cross-sectional cooling (Fig. 3c). Johns et al. (1995a) also reported that the Kuroshio was in its offshore position in March 1995 and onshore position in May 1995 based on their analysis of hydrographic section data.

In order to distinguish meandering and transport fluctuations and their preferred timescales, we calculate the spectrum of $\langle v' \rangle^2$ and $\langle v'^2 \rangle$, where, v' is the fluctuative velocity after deduction of the time mean, and the angle bracket denotes a cross-sectional average. Here $\langle v' \rangle^2$ is proportional to the square of fluctuating transport, whereas $\langle v'^2 \rangle$ is proportional to downstream component of eddy kinetic energy averaged across the channel. When currents across the section are equally varying and in phase, $\langle v' \rangle^2 = \langle v'^2 \rangle$. Large $\langle v'^2 \rangle$ but small $\langle v' \rangle^2$ would indicate a large degree of cancellation of the flow fluctuations over the cross section, suggesting the likelihood that energetic velocity fluctuations do not result in high transport variations. The spectra of $\langle v' \rangle^2$ and $\langle v'^2 \rangle$ of the Kuroshio measured by PCM-1 are shown in Fig. 4, illustrating that the strongest velocity fluctuations described by $\langle v'^2 \rangle$ are in frequency bands of 70–200 days, 25–40 days, 15–21 days, and 7–11 days. The v fluctuation spectrum ($\langle v'^2 \rangle$) is coincident with the transport spectrum ($\langle v' \rangle^2$) at the lower two bands (near 100 days and 30 days), indicating that the fluctuating v leads to transport variations at these particular period

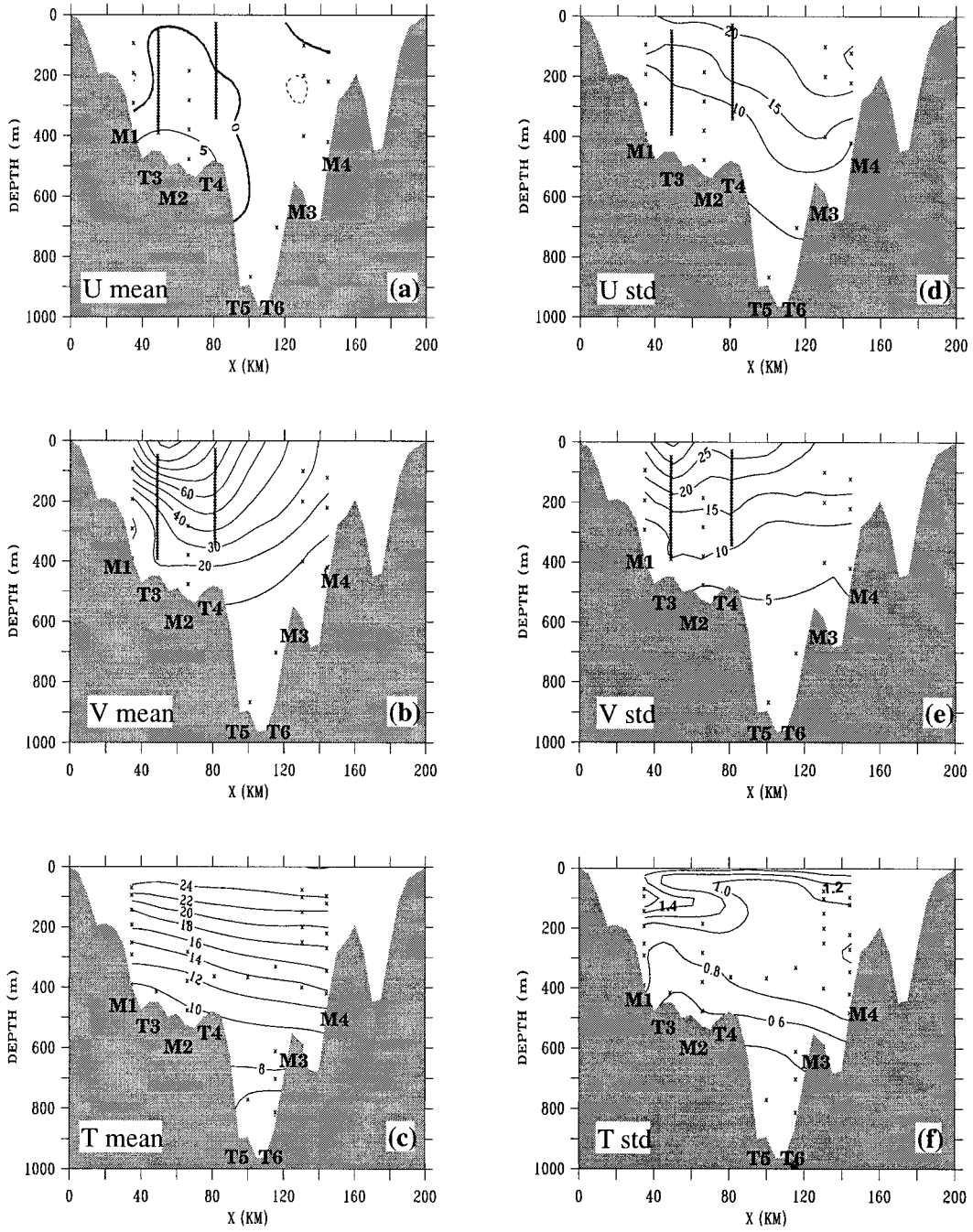

FIG. 2. Cross sections of averaged east (u) and north (v) velocity components and temperature (T), and the standard deviations of u, v, and T in the PCM-1 measurement period. Superimposed are the configurations of current and temperature measurements for velocity and temperature fields, respectively. (a) and (d) Calculations based on u measurements in period A (Sep 1994–May 1995).

bands. The still significantly smaller values of $\langle v' \rangle^2$ than $\langle v'^2 \rangle$ over these two bands, however, suggest that the cancellation effect described above is also present. This cancellation effect is more significant at the two higher-frequency bands (18 and 10 days), so the energetic fluctuating v does not result in strong transport variations.

4. EOF analysis

a. Time-domain EOF analysis

The foregoing section demonstrates complex structures of velocity and temperature and their variations in the ETC as observed by the PCM-1 moored array. Em-

TABLE 1. Parameters used in the objective analysis scheme.

C_1	0.95	correlation at zero lag
C_2	−0.06°long/day	east–west phase speed
C_3	0°lat/day	south–north phase speed
C_4	3.0°long	east–west zero-crossing scale
C_5	3.0°lat	south–north zero-crossing scale
C_6	2.0°long	east–west dacay scale
C_7	2.0°lat	south–north decay scale
C_8	20 day	temporal decay scale

pirical orthogonal function (EOF) analysis is useful to reduce the sample space to a smaller dimension and resolve the complex variance patterns of physical fields into dominant modes (Preisendorfer 1988). In this study, the v and T fields between M1 and M4 excluding the upper 100 m, which represent the best sampled part of the cross section, are used in the EOF analysis. In order to combine v-component and temperature fields, normalization was performed before calculating the covariance matrix, but redimensionalized rms structures for the EOFs will be shown.

Figures 5 and 6 display the first two EOF structures and principal component (PC) of the combined v and T fields. Together these two modes explain about 60% of the total variance. The first mode (hereafter referred to as the ''transport'' mode for convenience) accounts for 34% of the variance and can be described as a transport mode that represents transport pulses superimposed on the mean structure. This mode is characterized by in-phase variation of v across the channel with a core of largest amplitude situated at the mean velocity core position. The PC time series reasonably tracks the transport time series shown by Fig. 3b. Positive PC values of this mode indicate a pulse of increased flow and larger

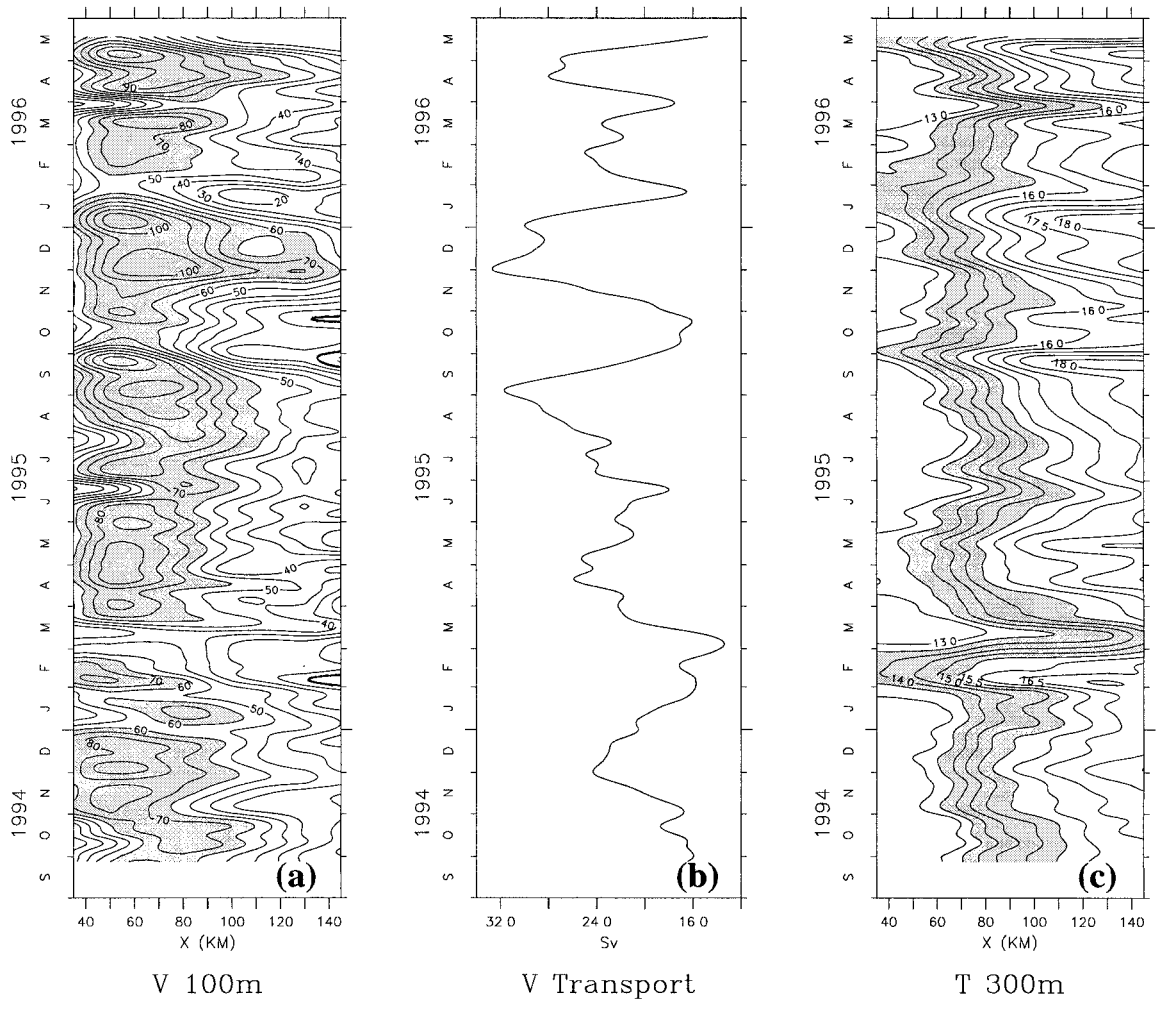

FIG. 3. Twenty-day low-pass-filtered time evolution of downstream velocity at 100 m (a), Kuroshio transport time series (b), and time evolution of temperature at 300 m (c). The shaded areas of (a) indicate downstream velocities greater than 60 cm s^{-1}. At 300 m, the temperature between 13.5° and 15.5°C is marked by the shaded band. Abscissas of (a) and (c) are distances from the east coast of Taiwan. The mean v (Fig. 2b) and T (Fig. 2c) structures suggest the lateral range of this temperature band can be an indicator of Kuroshio axis at 300 m.

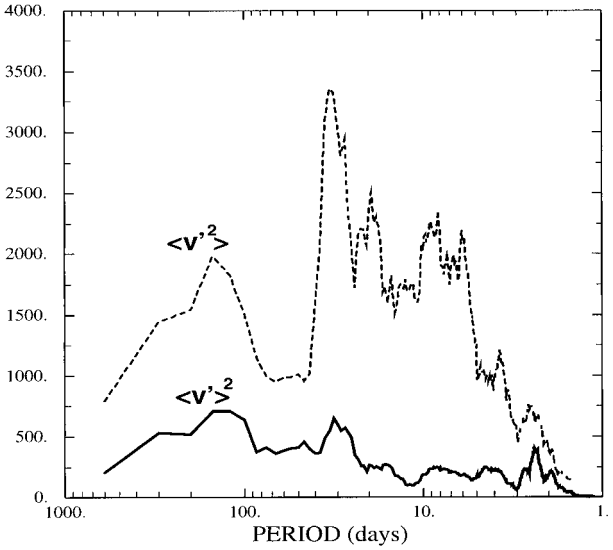

FIG. 4. Variance conserving spectra of $\langle v' \rangle^2$ and $\langle v'^2 \rangle$: overlapping time series of 601 days 1994–1996.

transport through the ETC, and vice versa. Consistent with this core is a significant thermal shear ($\partial T'/\partial x$) along the thermocline shown in Fig. 5b. The middepth core of highest T' indicates a greater depression of the thermocline in the east than in the west, leading to increased baroclinic shear of the Kuroshio. A steeper thermocline (larger $\partial T'/\partial x$) is indicative of higher baroclinic transport; a more level thermocline (smaller $\partial T'/\partial x$) is indicative of lower baroclinic transport. The first EOFs of v and T also indicate that positive (negative) transport anomalies tend to be accompanied by warm (cold) temperature anomalies across the entire section.

The second EOF (hereafter referred to as the ''meandering'' mode), explaining 25% of the variance, is dominated by meandering motions as indicated by the antiphase variation of the downstream velocity on either side of the mean current axis. A positive value of the PC for this mode represents an onshore meander of the current in the ETC. That the temperature anomalies increase from the western edge to the current and decrease toward the eastern part of the channel (reflecting $\partial T'/\partial x > 0$ in the west and $\partial T'/\partial x < 0$ in the east) is consistent with the out-of-phase variation of v EOF2. The time series of PC2 clearly demonstrates rapid and large onshore shifts of the Kuroshio axis. But the significant offshore meanders, such as those strongly suggested by the temperature field (Fig. 3c) in early March 1995, late June 1995, and the end of January 1996, are not so evident in the PC2 time series. Later on, we will use the frequency domain EOF analysis and the altimetry data to show that this is caused by the incomplete sampling of the current system by the PCM-1 array when the Kuroshio axis largely moves offshore.

The spectra of the first two PCs and their coherence with the total transport time series are shown in Fig. 7. Like the transport spectrum, the spectrum of the transport mode shows the dominant timescale of variability to occur in the period band 70–200 day. It also shows significant variabilities at periods near 28–40 days. The meander mode has three energy peaks at frequency bands of 12–22, 33–50, and 70–200 days. The peaks in both modes at the lowest two frequency bands are consistent with the spectra of $\langle v'^2 \rangle$ and $\langle v' \rangle^2$. The three energy peaks of the meandering mode are also strongly suggested by the $\langle v'^2 \rangle$ spectrum. The lack of a 7–11 day peak in the meandering mode spectrum while present in the $\langle v'^2 \rangle$ spectrum will be discussed later on.

Although the transport mode is coherent or marginally coherent with the transport time series over most of the frequency bands, they are incoherent in the periods of 12–22 days and 33–50 days, the periods at which the meandering mode is energetic. In the three most energetic meandering bands, there are secondary but insignificant coherence peaks in the cross-spectrum of the meander mode and the total transport (Fig. 7e). The reconstructed transport time series from the first two EOF modes is shown to be significantly coherent with the original transport time series over all frequency bands (Fig. 7f), indicating that Kuroshio meandering contributes to the variation of the transport into the ECS.

Note that these EOF modes, while orthogonal and hence uncorrelated in the time domain, are not necessarily uncorrelated in every given frequency band. Both transport and meandering modes possess high-energy peaks around 100 days and 30–40 days, suggesting that more variance may be explained by frequency-domain EOF analysis specific to these bands (see section 4b). Figures 3 and 6, if the not well-characterized offshore meanders in the PC2 time series are taken into account, generally show that the transport is low when the Kuroshio meanders offshore and high when the Kuroshio is in its onshore or normal position (as a western-intensified boundary current, the Kuroshio has a downstream velocity core in the western part of the channel close to the coast). Considering that the ETC serves as a choke point for the Kuroshio entering the ECS and is open at the southern end toward the Philippine Basin, it is certainly conceivable that meanders could directly influence the transport into the ECS when the Kuroshio axis moves offshore since part of the Kuroshio water may then bypass the ETC to the east of the Ryukyu Islands. As we will show next, the two modes are, in fact, closely related to each other in certain frequency bands (especially the 100-day band), and both of them appear to be linked to the Kuroshio meanders upstream of the PCM-1 array along the coast of Taiwan. A strong Kuroshio variability on 100-day timescale is also evident in the current meter measurements downstream in Tokara Strait (Feng et al. 2000). The more detailed meander structures on different timescales are described in section 4b, and the Kuroshio deflection process and its relationship to the Kuroshio large meanders upstream of the ETC are discussed in section 5.

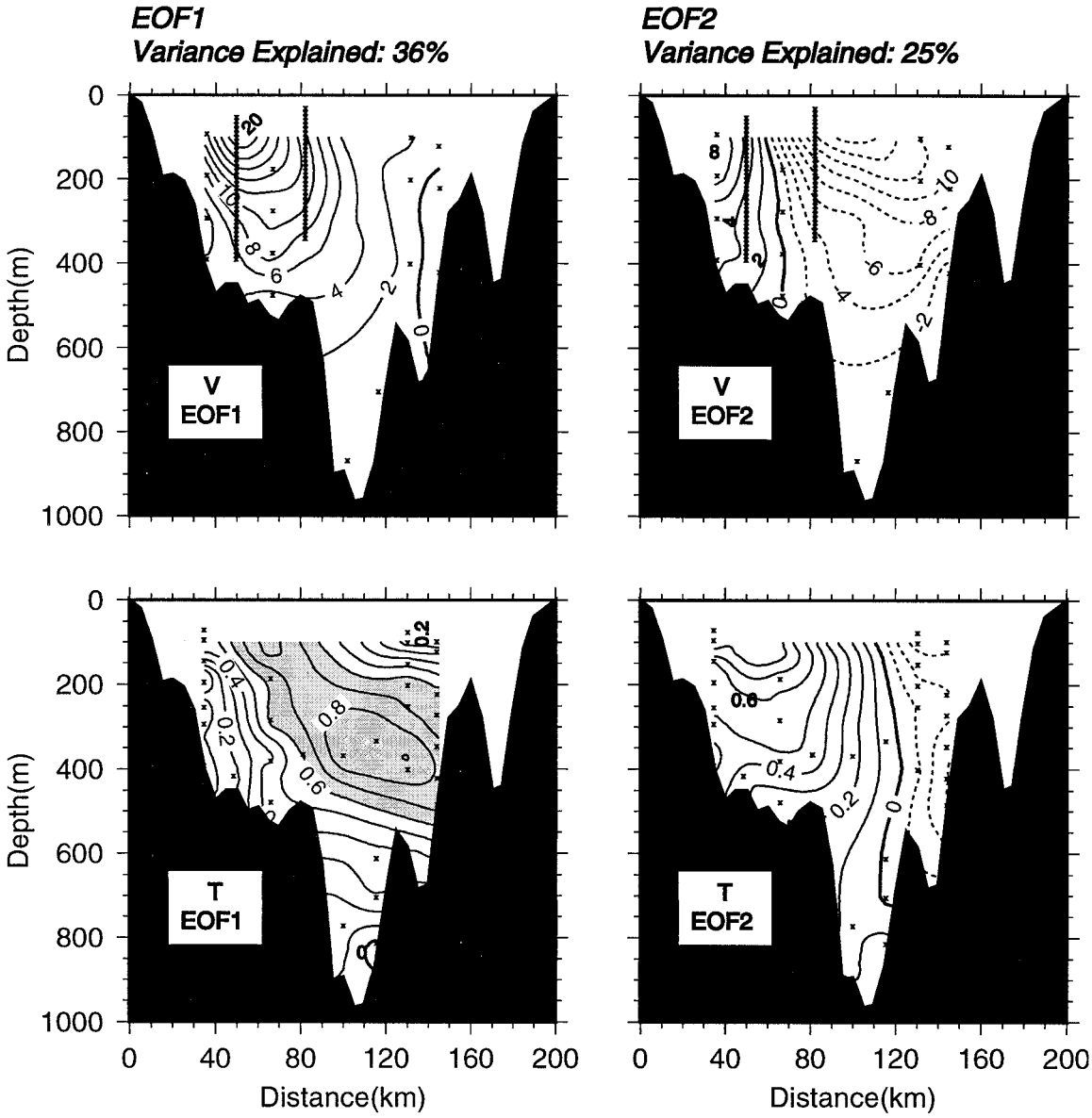

FIG. 5. Rms v-component and temperature fluctuations for the first two time-domain EOFs computed from the v-component and temperature covariance matrix.

b. Frequency-domain EOF analysis

The three energy peaks of the meandering mode in the time domain EOF analysis are consistent with the spectrum of $\langle v'^2 \rangle$ (Fig. 4), which also shows a fourth peak at period band of 7–11 days. To further elucidate the meander structure in the ETC, we will apply frequency-domain EOF analysis to the combined v and T fields at specific frequency bands of 70–200 days, 33–50 days, 12–22, and 7–11 days. The principle of the frequency-domain EOF analysis was originally described by Wallace and Dickinson (1972) and used on similar current meter array data in the Florida Current by Johns and Schott (1987). This analysis consists of computing the cross-spectral matrix for the set of observations, and the complex eigenvectors of the matrix. The cross-spectral matrix is the counterpart of the covariance matrix in the conventional time domain EOF analysis. Its elements are normalized by corresponding spectral levels to account for the large energy inhomogeneity over the array and different physical variables analyzed (v and T). The amplitude and phase information contained in each complex eigenvector describe the spatial structure of a coherent fluctuation at this specific frequency band in contrast to the time domain EOF analysis, which only demonstrates the in-phase or out-of-phase spatial structure of all the fre-

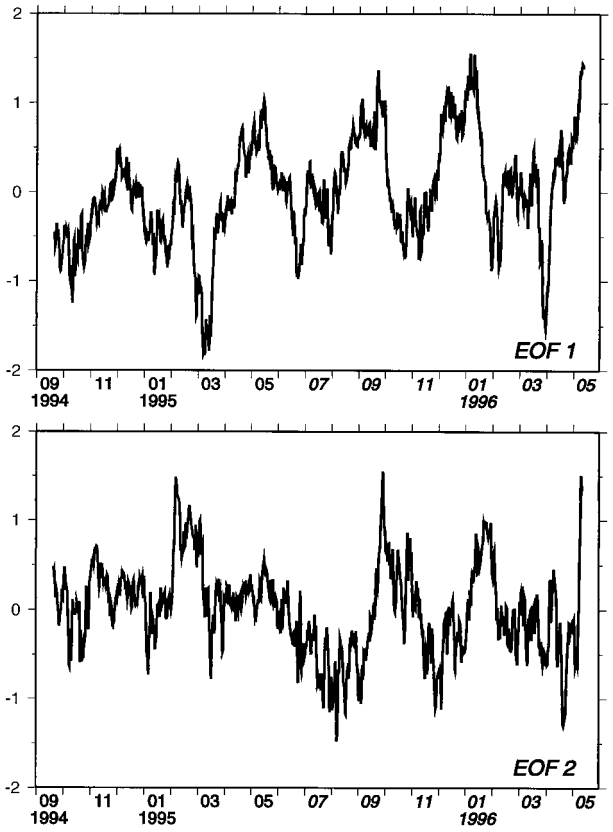

FIG. 6. The first two principal components of the time-domain EOF analysis from the v-component and temperature covariance matrix.

quency components. In the following we will identify the frequency-domain EOF as complex EOF (CEOF).

The first CEOF mode on the period band 70–200-days (Fig. 8a) explains about 72% of the total variance, suggesting that it extracts the major variation patterns in this band. It consists of a combination of the in-phase transport mode and out-of-phase meandering mode found in the time domain EOF analysis, both of which have spectral peaks in this band. The amplitude of v CEOF1 is more uniform horizontally than either of the previous time domain EOFs and the phase of v CEOF1 changes by 150° across the ETC. Physically, this corresponds to an increase or decrease of flow that sweeps westward across the channel (phase leading in the east). The 150° progressive phase change suggests that its ''out-of-phase'' node, if one exists, is located to the east of the ETC. This means that the lateral range of Kuroshio meanders is larger than the width of ETC and potentially part of the Kuroshio water can flow northward along the east of the Ryukyu Island chain. The amplitude of T CEOF1 also appears to result from a combination of the transport and meandering modes of the time domain EOF analysis. A meandering system whose current axis shifts onshore (offshore) without changing current strength should be associated with an in-phase cross-stream positive (negative) temperature anomaly. The basic feature in T CEOF1 phase structure is a 90° phase lead in the eastern part of the ETC, which corresponds to the main thermocline tilting and current strength and transport fluctuations due to both the transport and meandering variations. Explaining 55% and 42% of the total variance for the period bands of 33–50 days and 12–22 days, respectively, the CEOF1s (not shown) are similar to that for the band of 70–200 days in both amplitude and phase structures of v and T, except that the v amplitudes have smaller magnitude across the channel with a maximum core confined to the western part, and the v phase structures suggest that their associated lateral meandering ranges are comparable to the width of the ETC.

The first two time-domain EOFs do not suggest meandering in the frequency band of 7–11 days; however, this may be due to the strong out-of-phase cancellation of v fluctuations at this particular band as represented by Fig. 4. The CEOF1 in the period band 7–11 days explains about 33% of the total variance. This mode also exhibits meandering characteristics: it has a v' maximum in the western channel and a rapid 180° phase change through the mean Kuroshio downstream velocity core. Consistent with meandering, the maximum T variation also occurs in the western channel. Unlike the frequency bands of 70–200, 33–50, and 12–22 days, the associated T CEOF1 suggests no transport variation at the 7–11 day frequency band. The in-phase structure of the maximum T variation in the western channel also supports a ''pure meandering'' pattern within the 7–11 day frequency band. Because the meandering at this frequency band is confined to the western half of the channel and does not involve significant transport variation, its existence is not revealed by the first two time domain EOFs, which are associated with transport variations and meandering on a larger lateral range.

Except for the 7–11 day band meanders, the phase structures of T CEOF1 at the three other bands show that the T variations in the eastern side of the meander pattern always lead the western side by about 90°, which supports not only that there are baroclinic transport variations associated with those meanders but also that there is an apparent westward component of propagation along the PCM-1 array.

5. The 100-day fluctuations

According to the above EOF analyses, the dominant fluctuations of the Kuroshio within the ETC occur at periods near 100 days and contain a mixture of transport and meandering behavior. Further, frequency-domain EOF analysis over the 100-day band suggests the meandering amplitude is even larger than the array width, which means that the 100-day low transport pulses may arise from part of Kuroshio water shifting eastward to bypass the ETC. To understand the cause of the variability on the 100-day timescale, we investigate the spa-

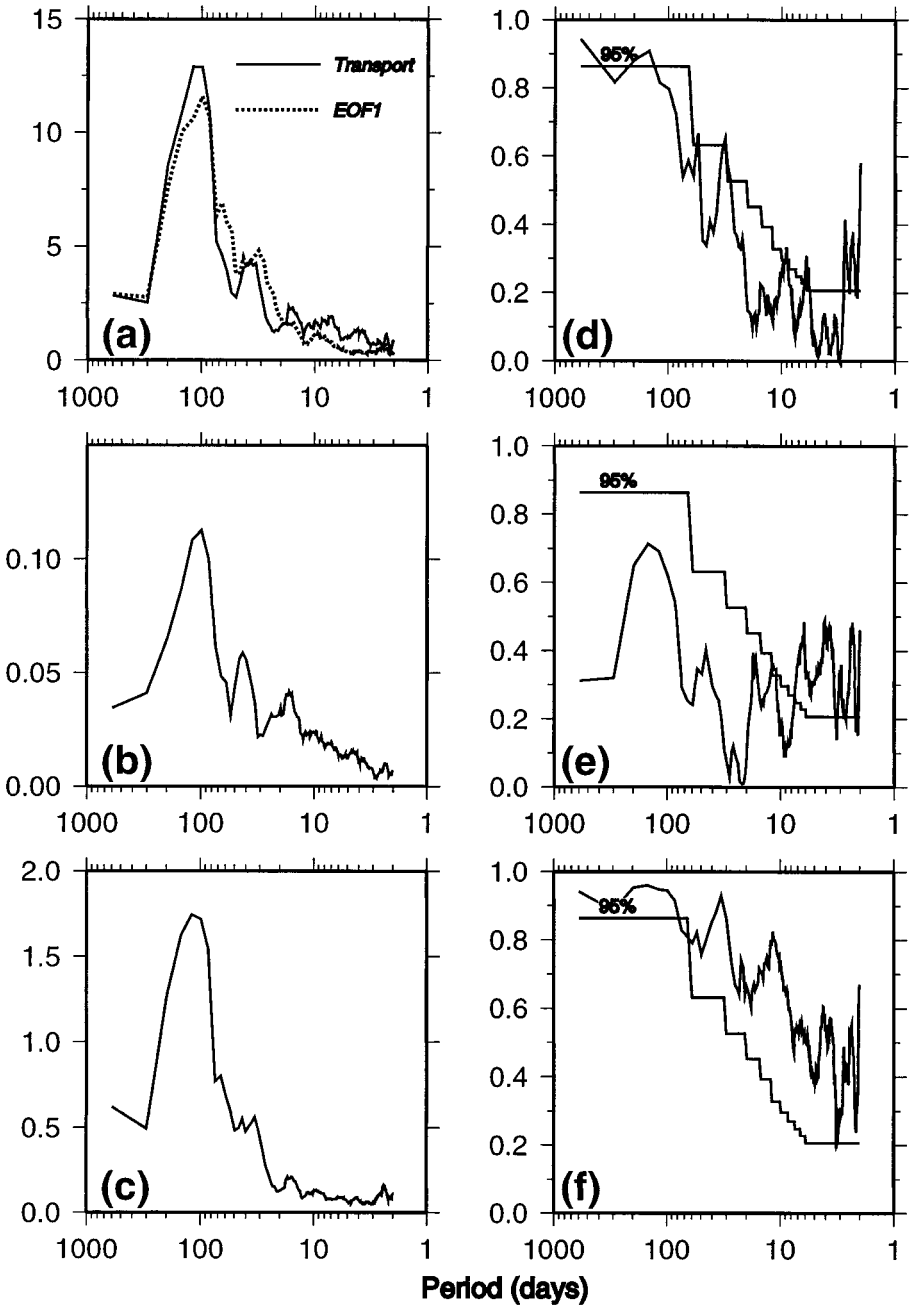

FIG. 7. The spectra of (a) Kuroshio transport and the first EOF (transport mode, scaled up to plot against the real transport), (b) the second EOF (meandering mode), and (c) the combination of the first two EOFs. The coherence square between the total transport and EOF1 (d), EOF2 (e), and the combination of the first two EOFs (f).

tial and temporal variations over a larger domain in the region using SSHA fields measured by T/P as well as some drifter observations.

A segment of T/P ground track 127 is parallel to the coast of Taiwan (Fig. 9). TOPEX/Poseidon flies over this segment every 9.92 days and can provide an estimate of the cross-track surface velocity anomaly on the basis of geostrophic balance. Before calculating the cross-track velocity anomaly, the alongtrack SSHA was smoothed by a 50-km running mean filter to reduce small-scale noise. The calculated cross-track velocity anomalies are plotted in Fig. 9 and are overlaid with velocity vectors at 200 m from the PCM-1 array for a sequence of meanders that correspond to a major low transport event occurring in March 1995. This event is characteristic of the 100-day low transport events as-

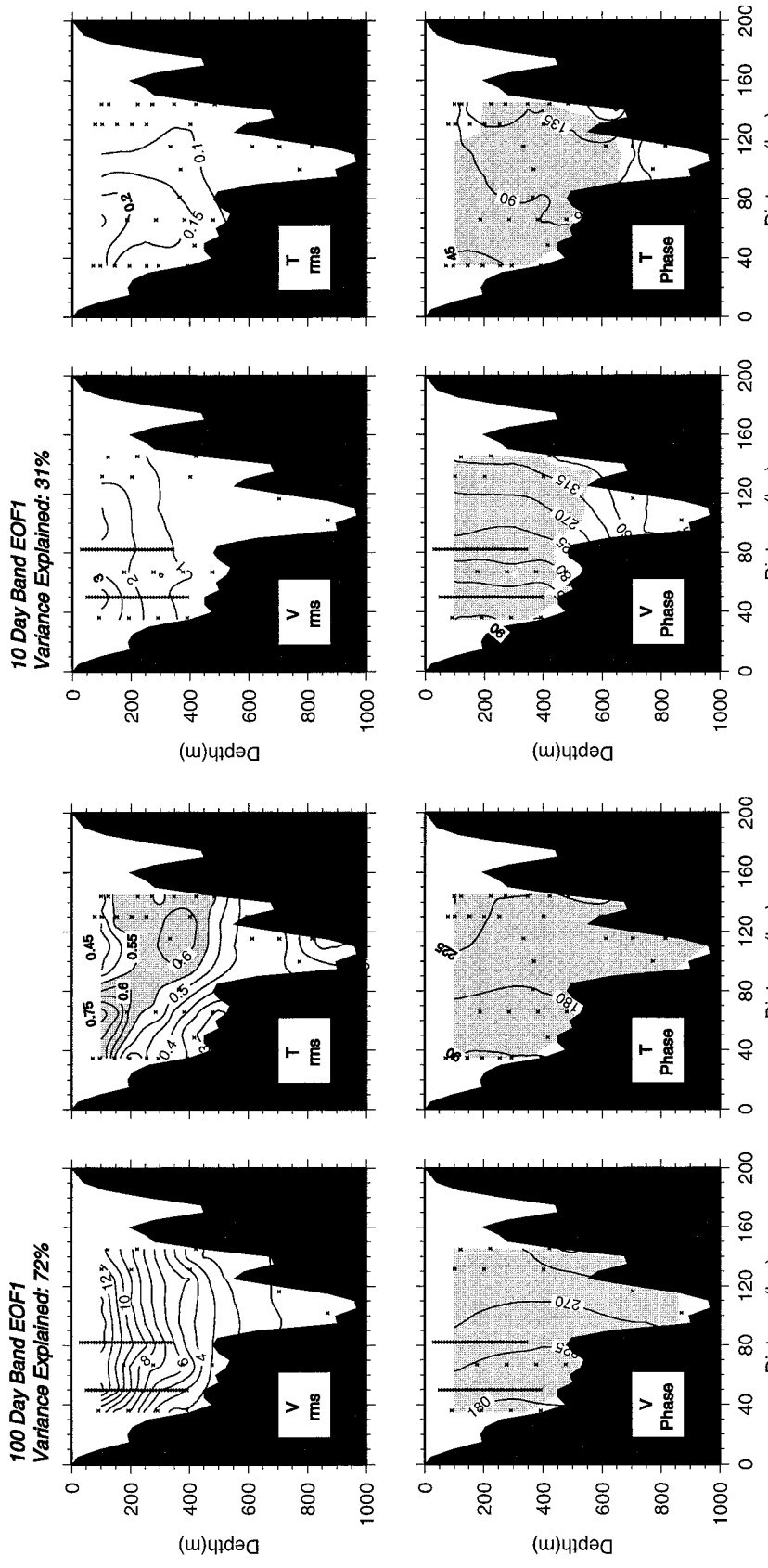

FIG. 8. (a) Contours of (upper panels) the first mode rms amplitude and (lower panels) phase of v and T frequency-domain EOF analysis over the PCM-1 array for the 100-day period band. Shaded regions in the phase plots indicate regions where the coherence of that variable with the mode is significant at 95% level, that is, where the mode accounts for a significant portion of the total signal. Rms of T larger than 0.55°C also shaded. (b) As in (a) but for the first mode in the 10-day band.

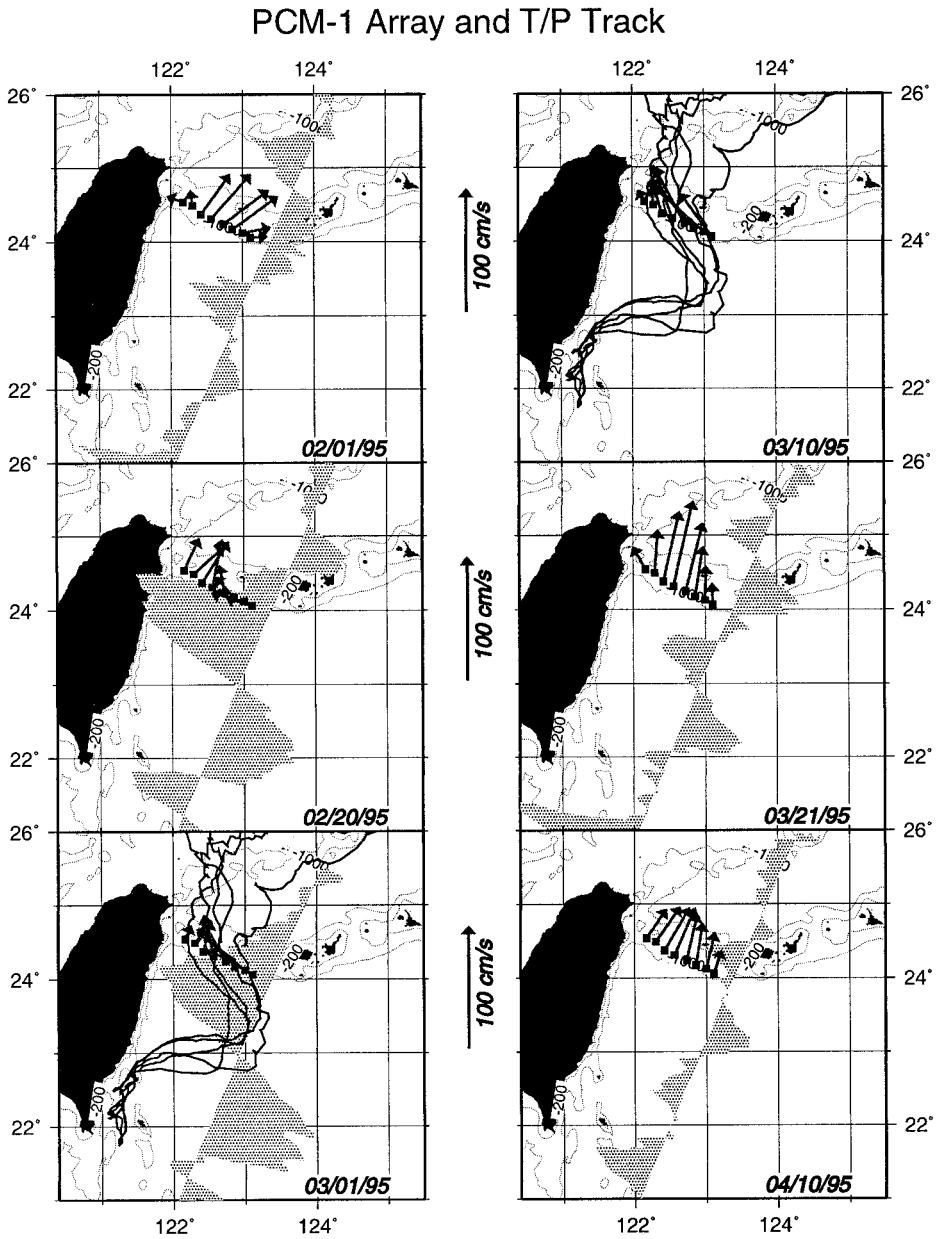

FIG. 9. Velocity vectors at 200 m and cross-track surface velocity anomalies derived from T/P altimetry along ground track 127, superimposed on the bathymetry contours (200 and 1000 m). The cross-track surface velocity anomaly is presented by gray shading (T/P failed to return data on 10 Mar 1995) using the same scale of the 200-m velocity vector in the ETC. The scale vectors of 100 cm s^{-1} are shown in the middle of the two columns. Five surface drifter trajectories are plotted in thick lines.

sociated with meandering that occurred several times in the record. Five surface drifter (drogue depth of 15 m) trajectories extracted from the NOAA/AOML WOCE surface drifter dataset (Hansen and Poulain 1996) are also shown in Fig. 9. These drifters were launched on 3 March 1995 near the southeast coast of Taiwan and passed through the PCM-1 array between 10–12 March 1995. These three independent datasets clearly show that the low transport of early March 1995 was caused by a large Kuroshio meander that shifted the axis offshore and changed the flow field from its normal northward direction perpendicular to the PCM-1 array to nearly westward and parallel to PCM-1. The sequence of events was as follows (see Fig. 9): On 1 February the Kuroshio flowed northeastward in its normal direction. On 20 February a large upstream meander that also carried cold water associated with the large meander trough began to cause westward flow in the eastern moorings. Between 1 and 10 March the ETC was dominated by a strong onshore flow with the meander trough

approaching, causing the Kuroshio to flow toward the shallow banks between the eastern mooring M4 and the southern tip of the Ryukyu Islands where depths are less than 200 m. These shallow banks effectively blocked part of the Kuroshio water from entering the ECS and induced the lowest downstream transport during this period. Note the strong offshore meander path of all five drifters during this period. Even though all five drifters went into the ECS, they were launched on the shoreward side (cyclonic side) of the Kuroshio, and one of them barely passed the eastern end of the channel over mooring M4. This suggests that water parcels in the anticyclonic side of the Kuroshio may have been forced to flow northward along the eastern side of the Ryukyu Islands. From 21 March to 10 April, the Kuroshio changed back toward its normal state.

To study the persistence of these large meanders and their general characteristics, a time-domain EOF analysis was performed on the cross-track surface velocity anomalies along T/P ground track 127 between the latitudes of the southern end of Taiwan and 24°N for the period October 1992–December 1997. The rms amplitude of the first EOF, which explains 40% of the total variance, is shown in Fig. 10a, indicating a meander pattern by the out-of-phase velocity anomalies to the north and south of 23°N. In agreement with the transport EOF mode spectra (Fig. 7) of v and T measured by the PCM-1 array, the spectra of the first PC (Fig. 10b) was characterized by a dominant energy peak in the 60–150 day band and a secondary peak at 20–40 days. This indicates a strong relationship between the transport fluctuations represented by in-phase cross-sectional v variations and the PCM-1 array upstream large meander.

Figure 11 displays the Kuroshio transport fluctuations (5-day low passed) and a latitude–time plot of objective analysis mapped SSHA from altimetry: the boxes from the bottom to the top display SSHA contours in the 18°–25°N latitude range at longitudes from 133°E to 124°E. In order to remove the steric height variations, the seasonal cycle (semiannual and annual harmonics) determined during the 1992 to 1997 T/P period was subtracted from the original SSHA. Westward propagating features are clearly identified from their time displacement in longitude (Fig. 11). The dominant westward propagating positive SSHA are signatures of anticyclonic eddies. The most energetic and clearly defined eddies are lined up and compared with Kuroshio transport fluctuations observed by the PCM-1 array. The slopes of these lines indicate the westward migration speed of these eddies to be approximately 10 km day^{-1} on average. It is interesting to note the near perfect timing between Kuroshio low transport pulses and the anticyclonic eddies approaching the western boundary south of PCM-1 array. These eddies merge/interact with the Kuroshio and develop the large offshore Kuroshio meanders upstream of the PCM-1 array that in turn steer part of the Kuroshio water to the east of the Ryukyu Islands. In constrast to the anticyclonic eddies, the cyclonic anomalies in our interest domain are less persistent. The cyclonic anomalies that can be clearly seen to the north of the anticyclonic anomalies along the east coast of Taiwan (124°E) appear to be locally generated and associated with the developed Kuroshio meanders. Figures 9 and 10 suggest that these cyclonic anomalies are corresponding to the crest of the Kuroshio meanders approaching the ETC. The time delay of the March 1995 low transport in responding to the eddy arrival at the

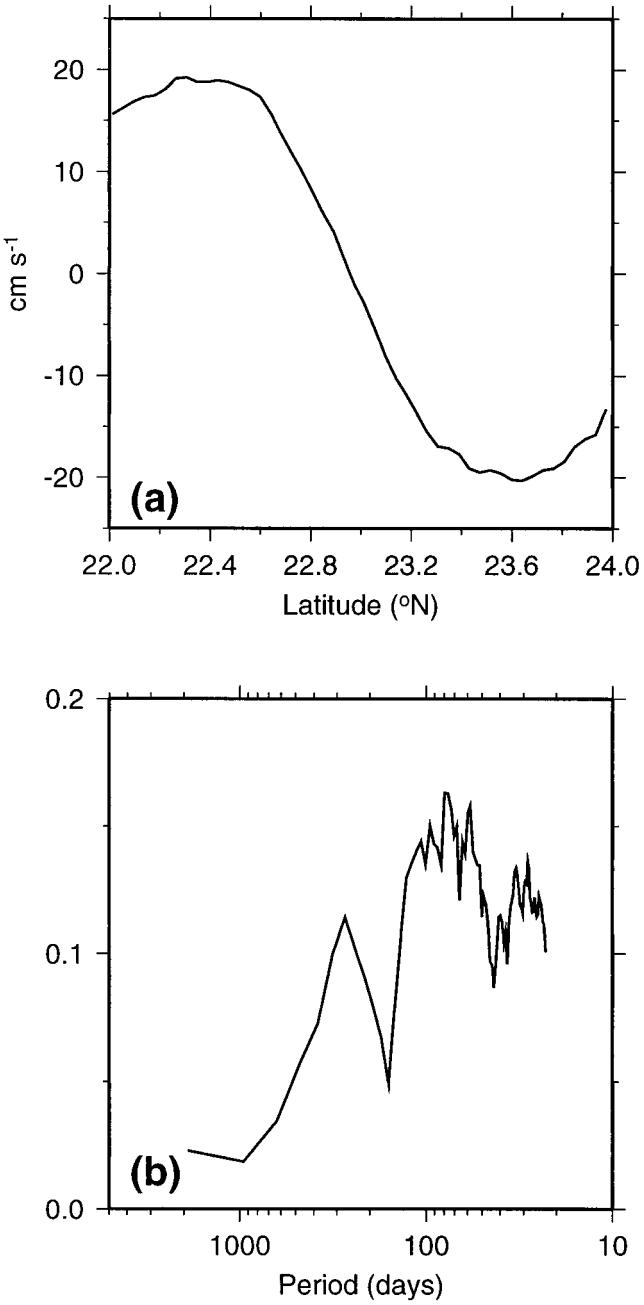

FIG. 10. Rms (a) and variance conserving spectrum (b) of the first mode of time-domain EOF for the cross-track surface velocity anomaly along TOPEX/Poseidon ground track 127 from 22° to 24°N.

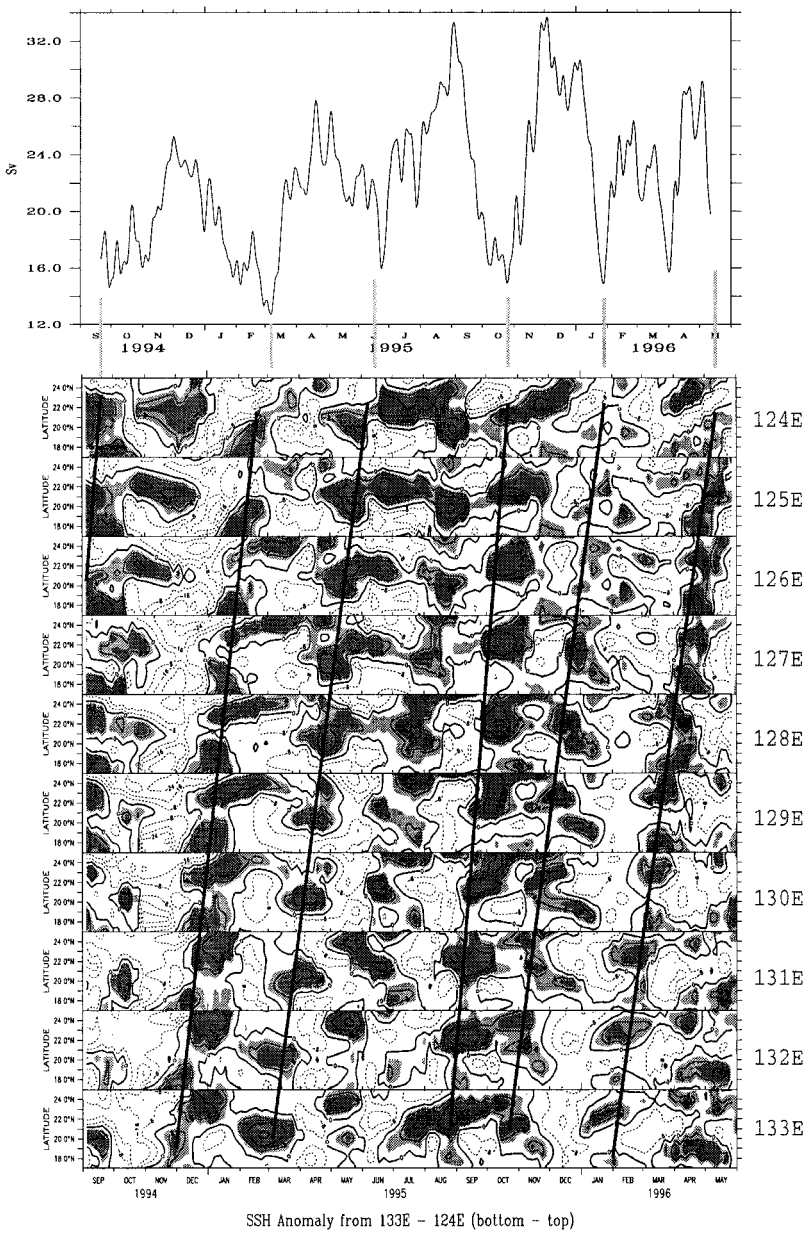

FIG. 11. Five-day low-passed Kuroshio transport time series measured by PCM-1 array (upper panel) and latitude–time plots of TOPEX/Poseidon sea surface height anomaly (SSHA) for longitudes 133°–124°E. The tilted lines indicate phase propagation of those features tracked from the interior ocean to the western boundary. The contour interval is 8 cm. The shaded area indicates the region where SSHA is larger than 5 cm, the darker area indicates SSHA larger than 10 cm.

western boundary can be explained by the time that the meander needed to propagate to the PCM-1 array site. The northward propagation of these meanders along 124°E can be identified from the northward tilt SSHA contours in the top latitude–time plot. Frequency-domain EOF analysis was performed on the OA mapped SSHA along 124°E, 125°E, 126°E, and 127°E meridians to the east of Taiwan (Fig. 12) at the frequency band 70–200 days. The first CEOFs confirm that the northward propagation can only be found near the western boundary along 124°E where the phase progressively changes by 160° from 20.5°N to 24°N. The mean northward propagation speed is estimated to be 9 ± 4 km day^{-1}. The rms of the CEOF1 is in agreement with a meander pattern (Fig. 10a) with a SSHA centered near 23°N.

In summary, the picture emerging from the above analysis is that arrival of westward-propagating anti-

cyclonic eddies to the south of the PCM-1 array from 18°N to 23°N can force a large Kuroshio meander to develop and these meanders can then result in the large 100-day transport fluctuations in the ETC by shifting the Kuroshio offshore and splitting part of the flow to the east of the Ryukyus. The sea level difference across the Kuroshio, which can be an indicator of the Kuroshio transport variation in the ETC (Johns et al. 2000), is also shown related to the sea level anomalies to the south of the ETC by Yang et al. (1999). While we cannot confirm that this splitting occurs from our available observations, it is shown in the next section that this is a characteristic feature of numerical model results that reproduce many of the same features seen in the PCM-1 array and altimetry data.

6. Comparison with numerical model results

The Parallel Ocean Climate Model (POCM), modified from the Semtner and Chervin ½° model (1992), has an average of ¼° resolution horizontally and 20 levels vertically in the global ocean. The unsmoothed topography was included through the introduction of the free surface scheme of Killworth et al. (1991). The model was initialized with results of an integration of 35 years from Levitus (1982) at ½° and a further 5-yr equilibration at ¼°. It was forced by 3-day averaged wind stress from daily European Centre for Medium-Range Weather Forecasts (ECMWF) 10-m winds and by monthly climatological surface heat flux obtained from ECMWF analyses (Barnier et al. 1995), in addition to a Haney (1971) T, S surface restoring term. The POCM model results have been compared to the T/P altimetry data and to the hydrography for WOCE sections, showing overall agreement with the observed large-scale mean circulation and its variability (Stammer et al. 1996; McClean et al. 1997). However, the model results were also shown to explain only 50% of the global T/P variability and hence underrepresent the eddy kinetic energy in the interior ocean. The 3-day sampled POCM model simulation in the western Pacific used in this paper was kindly provided by R. Tokmakian of the Naval Postgraduate School.

The POCM modeled v at 100 m and T at 200 m in the ETC across the PCM-1 array section and to the east to 125°E for v are shown in Fig. 13. The longitude of PCM-1 mooring M4 is 123.2°E. In comparison with the PCM-1 observations (Fig. 3), the most striking similarity is the significant fluctuation on 100-day timescales. The weak v pulses in the ETC are always accompanied by an increased v to the east of ETC, indicating increased Kuroshio water flow to the north along the eastern side of Ryukyu Islands during periods when the Kuroshio transport through ETC is significantly decreased (Fig. 15). The offshore shifts of the Kuroshio system in these low transport events can also be traced by the cross-sectional cold anomalies in the ETC.

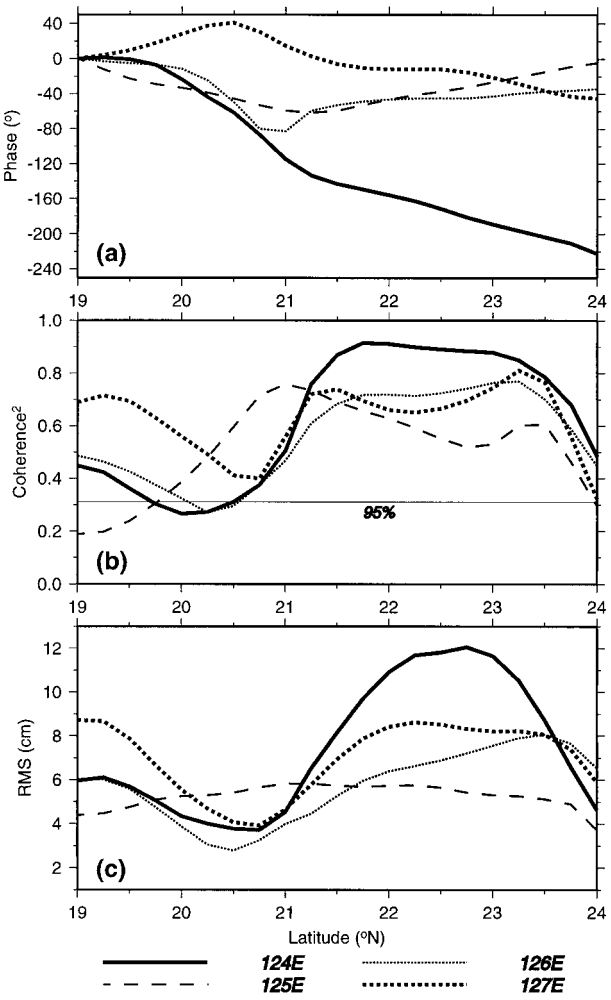

FIG. 12. (a) Phase, (b) coherence square, and (c) rms of the 1st frequency domain EOF of TOPEX/Poseidon sea surface height anomaly in the period band 100-day along meridians 124°, 125°, 126°, and 127°E. They explain 62%, 52%, 55%, and 63% of the total variance respectively. Also shown in the coherence plot is the 95% significant level. The phases along each meridian in (a) are referenced to 19°N.

The first two time-domain EOFs explain 43% of the total variance and reveal similar patterns (Fig. 14) to PCM-1 observations, with the first EOF (30% of variance) representing a transport mode and the second (13% of variance) a meandering mode. The spectrum of the modeled Kuroshio transport during the PCM-1 measurement period from September 1994 to May 1996 is plotted in Fig. 14b, showing the energetic 100-day fluctuations. The spectra (Fig. 14b) of both the modeled transport and meandering modes have 70–200-day energy peaks but no secondary peaks in the 18-day and 40-day bands, which is also indicated by Fig. 13. This underestimation in the higher frequency bands can also be found in the interior ocean as suggested by the globally averaged frequency–wavenumber spectrum of SSHA obtained from POCM and T/P altimeter measurement (Stammer et al. 1996). In their study, Stammer

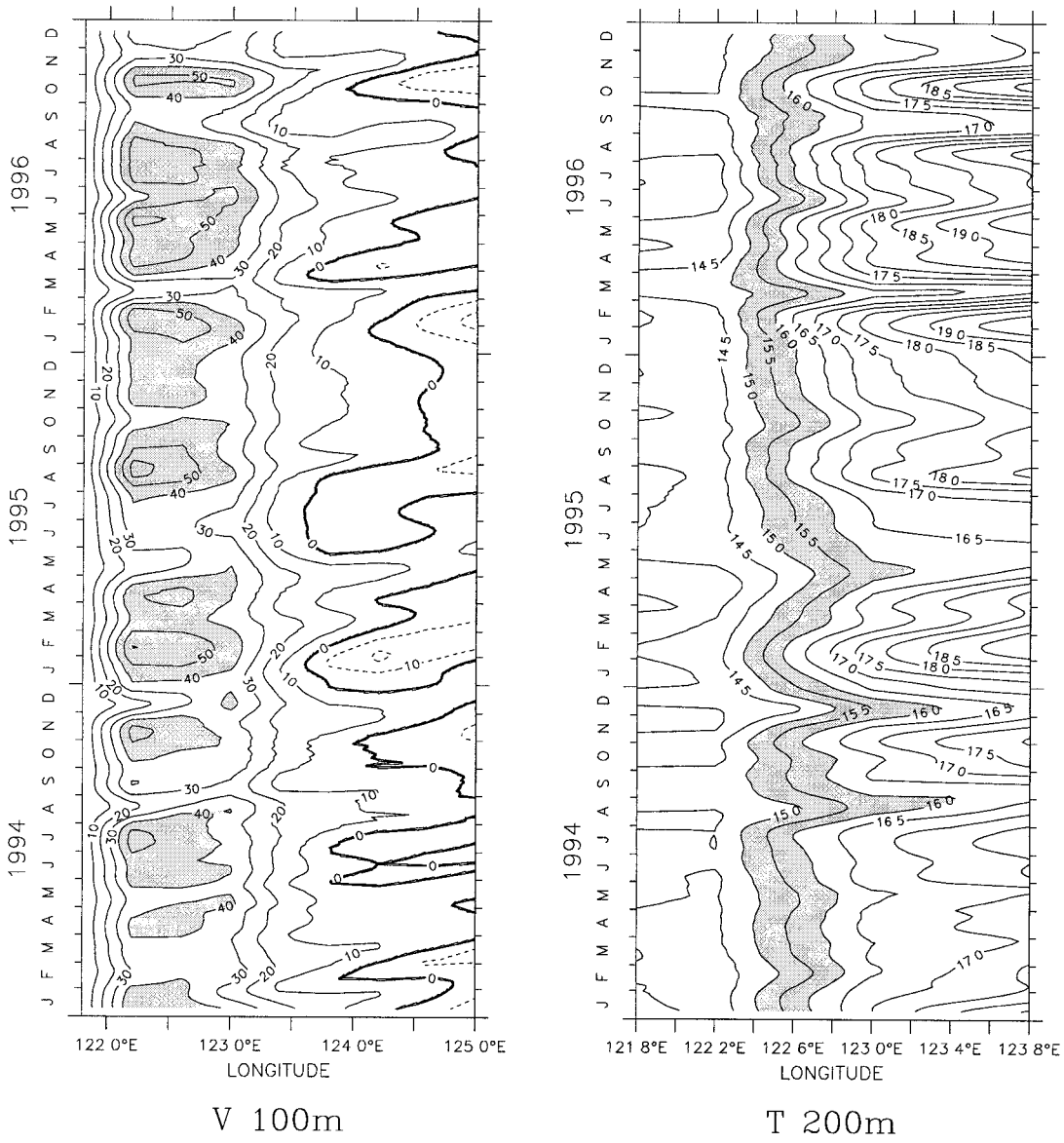

FIG. 13. 10-day low-pass filtered time evolution of downstream velocity at 100 m and temperature at 200 m, simulated by the Parallel Ocean Climate Model (POCM) for the period of 1994–96. Shaded areas show velocities larger than 40 cm s^{-1} and the temperature band between 15° and 16°C. The East Taiwan Channel ranges from 121.8°E to 123.6°E in the model.

et al. concluded that on timescales less than about a month and on space scales below 1500 km the model simulation significantly underestimates the variability presented in T/P data.

The top panel of Fig. 15 shows that the modeled Kuroshio transport in the ETC fluctuates on the 100-day timescale with an amplitude of 6–12 Sv, comparable to the PCM-1 observations, and that these transport fluctuations are generally compensated for by the northward transport in the 2° longitude band to the east of the Ryukyus at 24.3°N. The persistent westward propagating anticyclonic eddies are evident in the latitude–time plots of Fig. 15. Their propagating speed ranges from 6 to 12 km day^{-1}, in agreement with the T/P observations. The near perfect timing between the Kuroshio low transport events and the anticyclonic eddies approaching the western boundary again suggest that the 100-day Kuroshio transport variations in the ETC are associated with the arrival of westward propagating eddies from the interior ocean (Fig. 15), which lead to the Kuroshio large meanders steering part of the Kuroshio water flow northward to the east of the Ryukyus. That the weaker eddy kinetic energy in the model can still generate large Kuroshio transport in the ETC comparable to the observed may suggest that some other sources may help the Kuroshio meander development besides

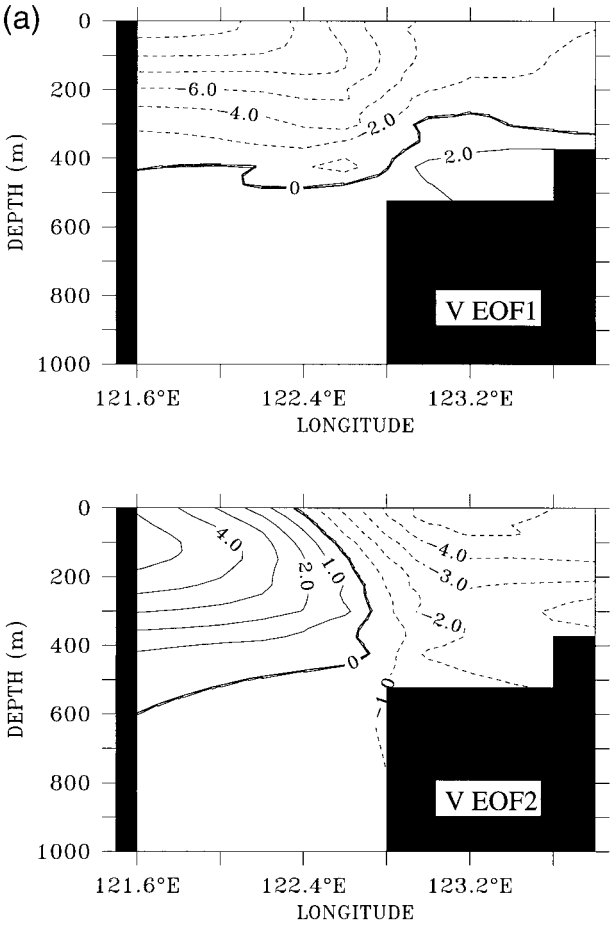

FIG. 14a. Rms v-component fluctuation of the first two time-domain EOFs computed from the POCM simulated v covariance matrix. Shaded regions indicate the model bottom topography.

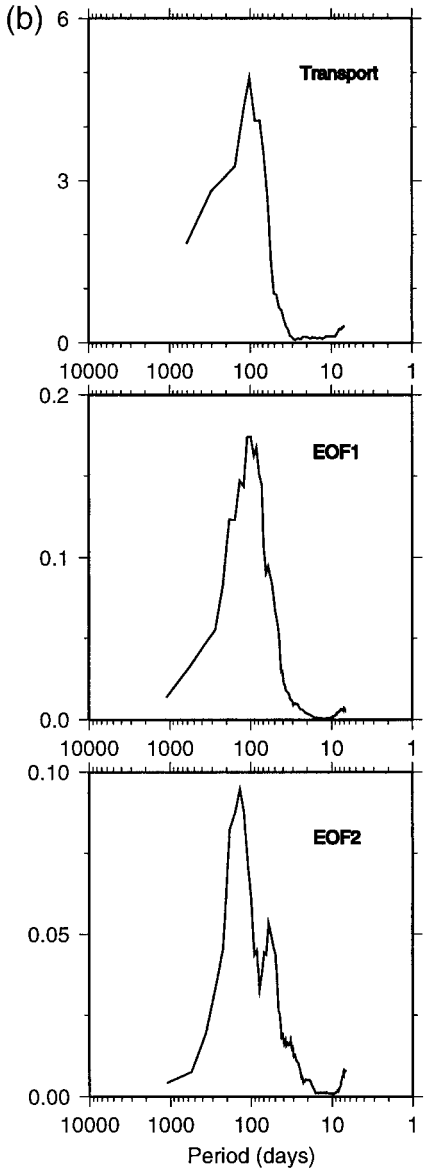

FIG. 14b. Variance conserving spectra of the POCM modeled Kuroshio transport during the PCM-1 measurement period from Sep 1994 to May 1996, and the first and second time-domain EOFs of modeled v components in the East Taiwan Channel during the 3-yr period of 1994–96.

the direct merger of the eddies with the Kuroshio. Calculation of the Reynolds interaction terms along the latitudinal sections south of the PCM-1 section suggests that the development of the large meanders, when the eddies arrive at the western boundary, may involve a barotropic instability process, where the largest energy trasfer comes from the interaction between the meridional velocity fluctuations and the downstream mean velocity shear in the meridional direction, that is,

$$\overline{v'v'}\frac{\partial\overline{v}}{\partial y}.$$

This is somewhat similar to the instability process to the east of the Bahamas in the Atlantic CME model reported by Böning et al. (1991).

7. Discussion and conclusions

In this paper, we have shown that the variations of the u, v, and T fields of the Kuroshio in the ETC are significant and that two basic structures related to coherent transport and meandering signals can be isolated in the PCM-1 array data using EOF analysis. The major variations of Kuroshio (about 60% of its variance) result

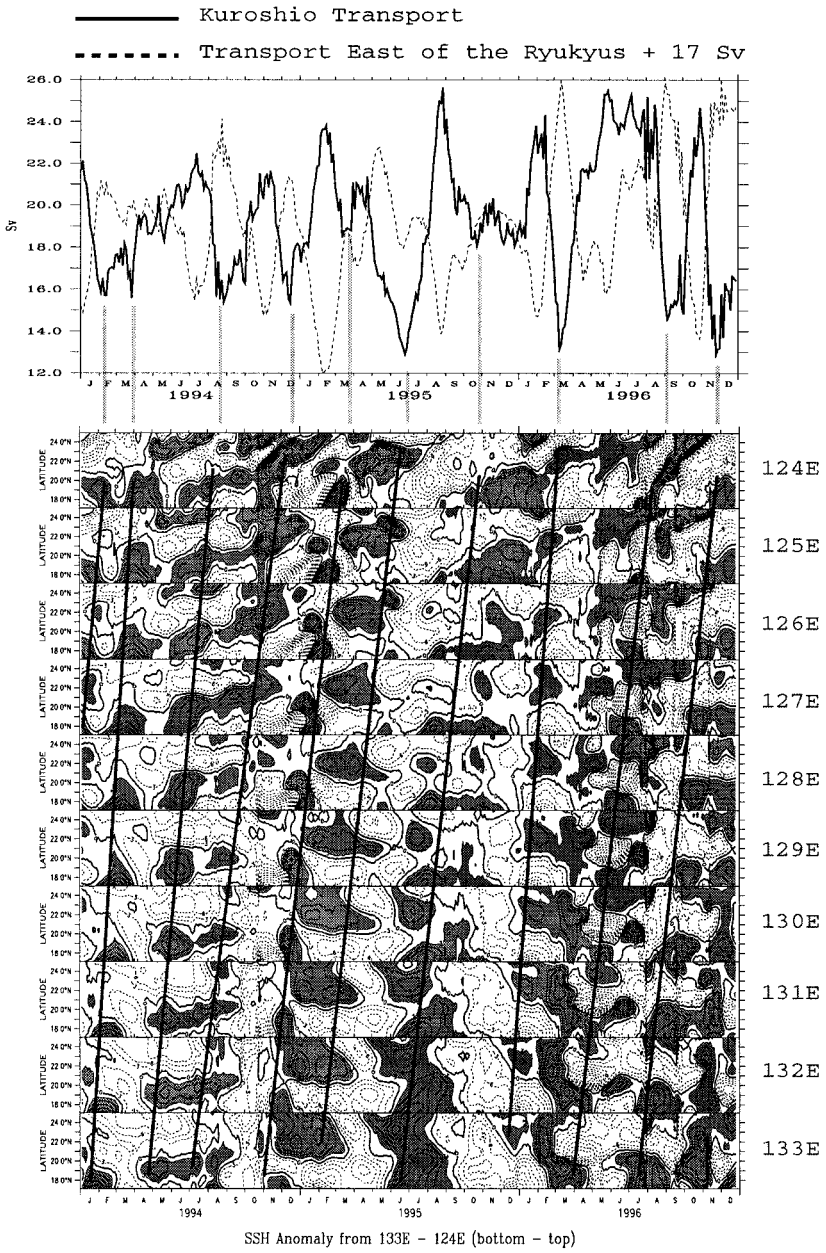

FIG. 15. Top: POCM modeled Kuroshio transport (solid line) and the northward transport between 124° and 126°E through 24.3°N (dashed line, added 17 Sv to be plotted against the Kuroshio transport time series). Bottom: A 3-yr latitude–time plot of SSHA for longitudes 133°–124°E computed from POCM. The contour interval is 3 cm. Shaded areas indicate the region where the SSHA is larger than 3 cm.

from a combination of the two modes, with the transport mode explaining the largest fraction (34%) of the total variability. The transport mode has a significant energy peak at 70–200 days, and a secondary peak near 30 days; the meandering mode is energetic over the periods of 12–22, 30–50, and 70–200 days. Spectral analysis of the Kuroshio transport and the first two principal components indicate the Kuroshio meanders at the three frequency bands are closely related to transport variations. This indication is further demonstrated by frequency-domain EOF analysis, which, in addition to the above three frequency bands, identified a higher frequency Kuroshio meandering band at periods of 7–11 days. The 7–11 day meanders are shown to be confined to the western part of ETC and involve little transport variation.

Due to the confinement of the Kuroshio flow by the ETC over the Ilan Ridge, the Kuroshio meanders at the

three lower frequency bands interact with the topography and induce transport variations through the ETC. This is consistent with the observations from available shipboard section data in the northern ECS, which show that the Kuroshio transport fluctuations propagate downstream at periods of 8–32 days (Ichikawa and Beardsley 1993). However, the moored transport time series showed the largest energy peak in the period band 70–200 days, as did the principal components of the transport and meandering modes. The phase structure of the frequency domain EOF analysis indicates the lateral range of the 70–200 day meanders is larger than the width of ETC and these large meanders appear to propagate downstream with the Kuroshio as suggested by the T/P altimeter data. The arrival of an offshore trough can shift the Kuroshio axis to the east end of the ETC and force a portion of Kuroshio water to bypass the ETC, flowing northward along the eastern side of the Ryukyu Islands. During these periods, the downstream transport is significantly reduced in the ETC as monitored by the PCM-1 moored array. POCM model results also show similar strong 100-day transport and meander variations in the ETC, and illustrate that the Kuroshio deflection to the east of Ryukyu Islands during the large meandering periods significantly reduces the transport through the ETC.

Both the T/P altimetry data and the POCM model simulation indicate that the 100-day meandering pattern is associated with the arrival of westward propagating mesoscale eddies from the western Pacific. The T/P measured rms of SSHA marks a regional maximum between 19° and 25°N, extending from the east of Taiwan to 175°W. The area-averaged eddy kinetic energy level for this region reaches half the eddy kinetic energy level of the Kuroshio Extension region. This band is coincident with the zone of surface eastward flow of the North Pacific Subtropical Countercurrent (STCC). Qiu (1999) attributes this regional maximum of eddy kinetic energy to baroclinic instability associated with the large vertical velocity shear between the STCC and the northern edge of the westward flowing North Equatorial Current in the subsurface layer. The presence of 70–150 day wavelike eddies in the western Atlantic at similar latitudes has been found and discussed by McWilliams (1976), Halliwell et al. (1991), Böning et al. (1991), and Lee et al. (1996), based on current meter mooring data, satellite SST, and numerical models.

As described by Johns et al. (2000), there are many similarities between the Kuroshio in the ECS and the Florida Current trapped in the Straits of Florida. In the case of the Florida Current, almost 50% of its variability can be described by the meandering and transport EOF modes with the meandering mode accounting for slightly larger variance. However, the Florida Current meandering is energetic in higher frequency bands centered near 5 days and 12 days (Johns and Schott 1987), and no significant 100-day fluctuation in the Florida Current transport has been observed. A major difference between variations of the Kuroshio in the ETC and Florida Current in the Straits of Florida can be explained by the topographic difference in the two areas. The Florida Current is more restricted by the Bahamas Islands and banks and the upstream Antilles Island Chain. The mesoscale features propagating from the interior ocean are therefore effectively blocked from interacting with the Straits of Florida, and the Florida Current does not contain the energetic features on the 100-day timescale. Indeed, strong 100-day variations are observed in the Antilles Current and deep western boundary current east of the Bahamas and have been linked to the arrival of the aforementioned wavelike eddies from the western Atlantic (Lee et al. 1996). In contrast, the ETC is open to the Philippine Basin to the south and southeast and therefore significant interaction can take place. South of the ETC, mesoscale eddies propagate into the western boundary, merge with the Kuroshio, and form the northward migrating meanders. These meanders can dramatically reduce the Kuroshio transport in the ETC by steering Kuroshio water to the east of the Ryukyu Islands.

The POCM simulation produces similar current patterns of the 100-day variations in the ETC and reveals a similar connection to westward propagating mesoscale eddies in the western Pacific. The ¼° global ocean model however still appears too coarse to resolve the higher-frequency variations of the Kuroshio in the ETC and ECS on timescales of less than a month.

Acknowledgments. This work was supported by the National Science Foundation through Grants OCE9302187 and OCE9818672. D. Zhang greatly appreciates the University of Miami's support through its generous award of the Koczy Fellowship. We are grateful to the two reviewers for their careful review and stimulating suggestions. We thank Brian Beckley of NASA Goddard Space Flight Center for his help in getting the TOPEX/Poseidon collinear sea level height data, and Robin Tokmakian of the Naval Postgraduate School for providing the POCM modeling results for comparison. The Ferret program developed by S. Hankin at NOAA/PMEL was invaluable for some of the analysis.

REFERENCES

Barnier, B., L. Siefried, and P. Marchesiello, 1995: Thermal forcing for a global ocean circulation model using a 3-year climatology of ECMWF analyses. *J. Mar. Syst.*, **6,** 363–380.

Bingham, F. M., and L. D. Talley, 1991: Estimates of Kuroshio transport using an inverse technique. *Deep-Sea Res.*, **38,** 521–545.

Böning, C. W., R. Doscher, and R. G. Budich, 1991: Seasonal transport variation in the western subtropical North Atlantic: Experiments with an eddy resolving model. *J. Phys. Oceanogr.,* **21,** 1271–1289.

Bryden, H. L., D. H. Roemmich, and J. A. Church, 1991: Ocean heat transport across 24°N in the Pacific. *Deep-Sea Res.,* **38,** 297–324.

Callahan, P., 1993: TOPEX/Poseidon NASA GDR user's handbook.

JPL Rep. D-8590, Rev. C, Jet Propulsion Laboratory, Pasadena, CA, 89 pp.

Feng, M., H. Mitsudera, and Y. Yoshikawa, 2000: Structure and variability of the Kuroshio Current in the Tokara Strait. *J. Phys. Oceanogr.,* **30,** 2257–2276.

Gilson, J., D. Roemmich, B. Cornuelle, and L.-L. Fu, 1998: Relationship of TOPEX/Poseidon altimetric height to steric height and circulation in the North Pacific. *J. Geophys. Res.,* **103,** 27 947–27 965.

Guan, B., 1981: Analysis of the variations of volume transports of the Kuroshio in the East China Sea. *Proc. Japan–China Symp. on Physical Oceanography and Marine Engineering in the East China Sea,* Special Report of Institute of Ocean Research, Shimizu, Japan, Tokai University, 118–137.

——, 1983: Analysis of the variations of volume transports of Kuroshio in the East China Sea. *Chinese J. Oceanol. Limnol.,* **1,** 156–165.

Halkin, D., and T. Rossby, 1985: The structure and transport of the Gulf Stream at 73°W. *J. Phys. Oceanogr.,* **15,** 1439–1452.

Halliwell, G. R., Jr., P. Cornillon, and D. A. Byrne, 1991: Westward-propagating SST anomaly features in the Sargasso Sea, 1982–88. *J. Phys. Oceanogr.,* **21,** 635–649.

Haney, R. L., 1971: Surface thermal boundary condition for ocean climate models. *J. Phys. Oceanogr.,* **1,** 241–248.

Hansen, D. V., and P.-M. Poulain, 1996: Quality control and interpolations of WOCE–TOGA drifter data. *J. Atmos. Oceanic Technol.,* **13,** 900–909.

Ichikawa, H., and R. C. Beardsley, 1993: Temporal and spatial variability of volume transport of the Kuroshio in the East China Sea. *Deep-Sea Res.,* **40,** 583–605.

James, C., M. Wimbush, and H. Ichikawa, 1999: Kuroshio meanders in the East China Sea. *J. Phys. Oceanogr.,* **29,** 259–272.

Johns, W. E., and F. Schott, 1987: Meandering and transport variations of the Florida Current. *J. Phys. Oceanogr.,* **17,** 1128–1147.

——, T. N. Lee, C.-T. Liu, and D. Zhang, 1995a: PCM-1 array monitors Kuroshio transport. *WOCE Notes,* **38** (3), 10–13. [Available from U.S. WOCE Office, Department of Oceanography, Texas A&M University, College Station, TX, 77843-3146.]

——, T. J. Shay, J. M. Bane, and D. R. Watts, 1995b: Gulf Stream structure, transport, and recirculation near 68°W. *J. Geophys. Res.,* **100,** 817–838.

——, T. N. Lee, D. Zhang, R. Zantopp, C. T. Liu, and Y. Yang, 2001: The Kuroshio east of Taiwan: Moored transport observations from the WOCE PCM-1 array. *J. Phys. Oceanogr.,* **31,** 1031–1053.

Killworth, P. D., D. Stainforth, D. J. Webb, and S. M. Paterson, 1991: The development of a free-surface Bryan–Cox–Semtner ocean model. *J. Phys. Oceanogr.,* **21,** 1333–1348.

Konaga, S., K. Nishiyama, and H. Ishizaki, 1980: Geostrophic transport in the East China Sea and southeast of Yakushima Island—A case study. *Oceanogr. Mag.,* **31,** 33–44.

Leaman, K., R. Molinari, and P. Vertes, 1987: Structure and variability of the Florida Current at 27°N: April 1982–July 1984. *J. Phys. Oceanogr.,* **17,** 565–583.

Lee, T. N., J. A. Yoder, and L. P. Atkinson, 1991: Gulf Stream eddy influence on productivity of the Southeast U.S. continental shelf. *J. Geophys. Res.,* **96,** 22 191–22 206.

——, W. E. Johns, R. Zantopp, and E. Fillenbaum, 1996: Moored observations of western boundary current variability and thermohaline circulation at 26.5°N in the subtropical North Atlantic. *J. Phys. Oceanogr.,* **26,** 962–983.

Levitus, S., 1982: *Climatological Atlas of the World Ocean.* NOAA Prof. Paper No. 13, U.S. Govt. Printing Office, 173 pp.

Liu, C.-T., S.-P. Cheng, W.-S. Chuang, Y. Yang, T. N. Lee, W. E. Johns, and H.-W. Li, 1998: Mean structure and transport of Taiwan Current (Kuroshio). *Acta Oceanogr. Taiwan,* **36,** 159–173.

Mariano, A. J., and O. B. Brown, 1992: Efficient objective analysis of dynamical heterogeneous and nonstationary fields via the parameter matrix. *Deep-Sea Res.,* **39,** 1255–1271.

McClean, J. L., A. J. Semtner, and V. Zlotnicki, 1997: Comparisons of mesoscale variability in the Semtner–Chervin ¼° model, the Los Alamos Parallel Ocean Program ⅙° model, and TOPEX/Poseidon data. *J. Geophys. Res.,* **102,** 25 203–25 226.

McWilliams, J. C., 1976: Maps from the Midocean Dynamics Experiment. Part I: Geostrophic streamfunction. *J. Phys. Oceanogr.,* **6,** 810–827.

Miller, J. L., and T. N. Lee, 1995: Gulf Stream meanders in the South Atlantic Bight 1. Scaling and energetics. *J. Geophys. Res.,* **100,** 6687–6704.

Molinari, R. L., W. D. Wilson, and K. Leaman, 1985: Volume and heat transports of the Florida Current: April 1982 through August 1983. *Science,* **227,** 295–297.

Nitani, H., 1972: Beginning of the Kuroshio. *The Kuroshio,* H. Stommel and K. Yoshida, Eds., University of Washington Press, 129–163.

Preisendorfer, R., 1988: *Principal Component Analysis in Meteorology and Oceanography.* Elsevier, 425 pp.

Qiu, B., 1999: Seasonal eddy field modulation of the North Pacific Subtropical Countercurrent: TOPEX/Poseidon observation and theory. *J. Phys. Oceanogr.,* **29,** 2471–2486.

——, T. Toda, and N. Imasato, 1990: On Kuroshio front fluctuations in the East China Sea using satellite images and in situ observational data. *J. Geophys. Res.,* **95,** 18 191–18 204.

Roemmich, D., and T. McCallister, 1989: Large scale circulation of the North Pacific Ocean. *Progress in Oceanography,* Vol. 22, Pergamon, 171–204.

Schmitz, W. J., Jr., and W. S. Richardson, 1968: On the transport of the Florida Current. *Deep-Sea Res.,* **15,** 679–693.

Schott, F., T. N. Lee, and R. Zantopp, 1988: Variability of structure and transport of the Florida Current in the period range of days to seasonal. *J. Phys. Oceanogr.,* **18,** 1209–1230.

Schrama, E. J. O., and R. D. Ray, 1994: A preliminary tidal analysis of TOPEX/Poseidon altimetry. *J. Geophys. Res.,* **99,** 24 799–24 808.

Semtner, A. J., Jr., and R. M. Chervin, 1992: Ocean general circulation from a global eddy-resolving model. *J. Geophys. Res.,* **97,** 5493–5550.

Stammer, D., R. Tokmakian, A. J. Semtner, and C. Wunsch, 1996: How well does a ¼° global circulation model simulate large-scale oceanic observations? *J. Geophys. Res.,* **101,** 25 779–25 811.

Wallace, J. M., and R. E. Dickinson, 1972: Empirical orthogonal representation of time series in the frequency domain. Part I: Theoretical considerations. *J. Appl. Meteor.,* **11,** 887–892.

Yang, Y., C. T. Liu, J. H. Hu, and M. Koga, 1999: Taiwan Current (Kuroshio) and impinging eddies. *J. Oceanogr.,* **55,** 609–617.